A two-phase diffuse-interface model for Hele–Shaw flows with large property contrasts

Y. Sun [a], C. Beckermann [b,*]

[a] Department of Mechanical Engineering, State University of New York at Binghamton, Binghamton, NY 13902, USA
[b] Department of Mechanical and Industrial Engineering, The University of Iowa, Iowa City, IA 52242, USA

ABSTRACT

A novel two-phase diffuse-interface model is used to simulate flows inside a Hele–Shaw cell. The model assumes that the two phases coexist inside the diffuse interface, with different velocities and properties. A separate equation is used to calculate the slip velocity between the two phases inside the diffuse interface. It is shown that for one-dimensional flows parallel to the diffuse interface, the results are independent of the diffuse-interface width, regardless of the magnitude of the density and viscosity contrasts between the phases. This two-phase approach is coupled with a phase-field equation for calculating the interface motion. The model is applied to a buoyancy-driven two-phase flow involving a Rayleigh–Taylor instability and validated through a comparison with available sharp-interface results. The flows and interface topology changes are investigated for large density and viscosity contrasts between the phases. The convergence of the results with respect to the interface width is examined in detail. It is shown that the two-phase model converges better than a standard diffuse-interface model that assumes the presence of a single velocity inside the diffuse interface. Remaining interface width dependencies can be attributed to the capillary stress term in the momentum equation.

© 2008 Elsevier B.V. All rights reserved.

1. Introduction

Two-phase flows featuring topology transitions and other interface singularities have become an area of increasing research interest over the last decade [1–6]. In such flows, multiple length and time scales emerge and capillary stresses cannot be neglected. In the presence of interface singularities, conventional sharp-interface models fail to work and/or are difficult to solve numerically. Diffuse-interface approaches have been proposed to overcome these difficulties [1,6–8]. In diffuse-interface models, the interface is viewed as a region of finite extent over which the physical quantities vary in a rapid but smooth manner between the bulk fluid values. Of central importance in diffuse-interface models for fluids is the concept of a capillary stress tensor that describes the variation of the forces inside of the interface due to surface tension [6]. Aside from the issue of interface singularities, diffuse-interface models have become popular tools in the computation of large-scale two-phase flows featuring complex interface motions [6]. This can be attributed to the fact that a single set of governing equations is solved in both fluids and no special procedures are needed for satisfying interface conditions. However, in such computations the diffuse-interface width must usually be chosen much larger than the actual width, which is on the order of a few atomic dimensions. Hence, it is important to examine the dependence of the results on the diffuse-interface width.

All diffuse-interface models that are based on thermodynamic or continuum theories assume the existence of a single velocity and pressure at any point inside the diffuse interface. Usually, the fluid density (or composition for a binary fluid) is used as an order parameter to distinguish between the phases. For large property contrasts between the phases, standard diffuse-interface models can give results that are very dependent on the choice of the interface width [8]. Furthermore, the solution depends strongly on the variations of the density and viscosity across the diffuse interface, and these variations are often not uniquely defined by the theories [9]. In order to alleviate these difficulties, Sun and Beckermann [8] recently proposed a so-called "two-phase" diffuse-interface model. As opposed to diffuse-interface models that are based on thermodynamic or continuum theories, the two phases are assumed to coexist inside the diffuse interface with different velocities (i.e., there is a velocity "slip"), pressures and properties, while still accounting for the capillary stresses due to surface tension. The so-called phase-field, ϕ, instead of the density, is used as the order parameter to distinguish between the phases. The phase-field is viewed as an atomic-scale phase volume fraction and varies in a steep

---

* Corresponding author. Tel.: +1 319 335 5681; fax: +1 319 335 5669.
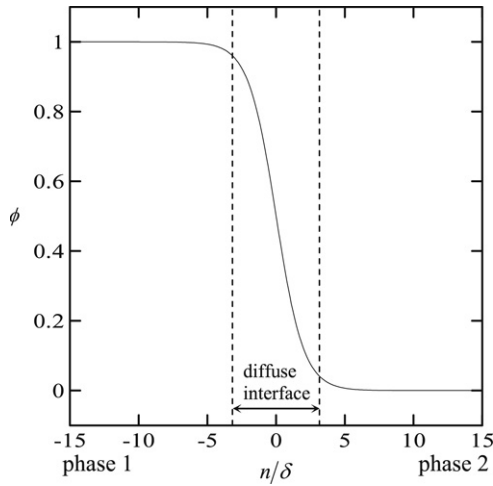*E-mail address:* becker@engineering.uiowa.edu (C. Beckermann).

Fig. 1. The diffuse interface and the phase field variation normal to the interface.

but smooth fashion across the diffuse interface, as shown in Fig. 1. Fig. 2 provides a simple illustration of the underlying differences between the two-phase model and standard diffuse-interface models that are based on thermodynamic or continuum theories, and of how both models contrast with the standard sharp-interface description of two-phase flows. Since standard diffuse-interface models treat all physical quantities inside the diffuse interface as single variables, they are also referred to in the following as "mixture" models. Diffuse-interface models can be related to the standard sharp-interface description in the limit of the interface width approaching zero. One important consequence of allowing for a velocity slip between the two phases in the two-phase model is that the solution for simple shear flows is *independent* of the interface width, regardless of the magnitude of the viscosity or density contrast between the two fluids [8]. This allows for the use of artificially large interface widths and hence significantly improves computational efficiency. Furthermore, since the properties and velocities in the two-phase model are defined separately for each phase, they do not undergo

the steep variations inside of the diffuse interface that are typically encountered in mixture models. However, in the presence of surface tension, the capillary stress still induces large pressure variations inside of the diffuse interface, and this is one of the issues investigated in the present study.

The two-phase diffuse-interface model was derived in Ref. [8] in the context of flows that are governed by the full Navier–Stokes equations. Many of the issues important in diffuse-interface models, such as interface width dependencies, can be better examined for more simple flows where inertia and other effects are not present and the governing equations are solved more easily. Thus, the present study is concerned with the application of the two-phase diffuse-interface model of Ref. [8] to large-scale Hele–Shaw flows that feature complex interface motions. Such Hele–Shaw flows have also been used by Folch et al. [4,5] and Lee et al. [2,3] to investigate the performance of various diffuse-interface models. Folch et al. [4,5] developed a thin-interface analysis to improve the accuracy and computational efficiency of their phase-field model for large viscosity contrasts, while Lee et al. [2,3] treated the two fluids as a binary (Cahn–Hilliard) fluid and used composition as the order parameter. In the present study, the performance of the two-phase diffuse-interface model of Ref. [8] is examined and comparisons are made with standard (mixture) diffuse-interface and sharp-interface descriptions. Particular emphasis is placed on the effects of large density and viscosity contrasts between the two fluids.

2. Governing equations

Before presenting the governing equations for the diffuse-interface model, the standard sharp-interface description of two-phase Hele–Shaw flow is reviewed. The phase-field equation is discussed last in this section.

2.1. Sharp-interface model

Consider the flow of two incompressible, immiscible fluids inside a Hele–Shaw cell. In the context of the present study utilizing the phase-field method, the two fluids are also referred
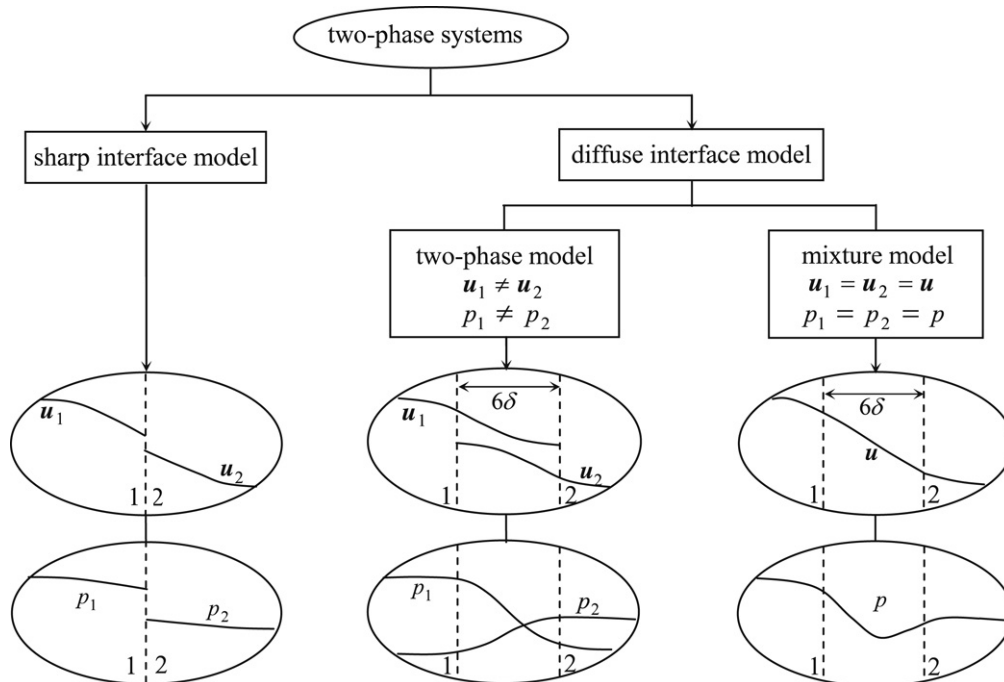

Fig. 2. Illustration of the sharp-interface, and two-phase and mixture diffuse-interface approaches.
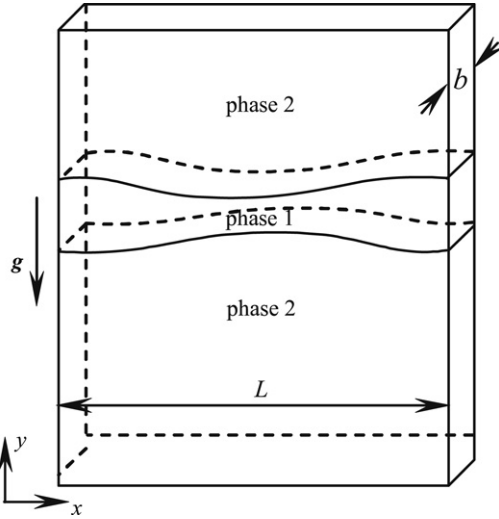
Fig. 3. Schematics of the two-phase Hele–Shaw cell problem.

to as phases and the subscript k (with $k = 1, 2$) is used to denote a phase. The density and viscosity of each phase are given by ρ_k and μ_k, respectively, and are assumed constant. The interfacial tension between the two phases is given by σ. As illustrated in Fig. 3, the Hele–Shaw cell has a gap of width b that is much smaller than the cell length L (i.e. $b \ll L$). Assuming no-slip boundary conditions at both surfaces forming the narrow gap and a parabolic velocity profile across the gap, the standard sharp-interface description for two-phase Hele–Shaw flows is given by [11]

Phase k

$$\nabla \cdot \mathbf{u}_k = 0 \tag{1}$$

$$\mathbf{u}_k = -\frac{b^2}{12\mu_k} \left(\nabla p_k - \rho_k \mathbf{g} \right) \tag{2}$$

Interface

$$(\mathbf{u}_1 - \mathbf{u}_2) \cdot \mathbf{n} = 0 \tag{3}$$

$$p_1 - p_2 = \sigma \kappa \tag{4}$$

where $\mathbf{u}_k$ and p_k are the gap averaged velocity and pressure of phase k, $\mathbf{g}$ is the gravitational acceleration, $\mathbf{n}$ is the interface unit normal vector pointing outward of phase 1, and κ is the interface curvature (positive when the interface is convex toward phase 2).

2.2. Diffuse-interface model

The diffuse-interface model of Ref. [8] assumes a certain stationary phase-field profile across the diffuse interface, which in the present study is taken to be the hyperbolic tangent function

$$\phi = \frac{1}{2} \left[1 - \tanh \left(\frac{n}{2\delta} \right) \right] \tag{5}$$

where n is the coordinate normal to the interface and δ is a measure of the diffuse-interface width. As shown in Fig. 1, ϕ varies from unity in phase 1 to zero in phase 2 over a distance of approximately 6δ. For the above profile, the interface curvature, κ, can be expressed as [8,10]

$$\kappa = \nabla \cdot \mathbf{n} = -\nabla \cdot \left(\frac{\nabla \phi}{|\nabla \phi|} \right)$$

$$= -\frac{1}{|\nabla \phi|} \left[\nabla^2 \phi - \frac{\phi (1 - \phi)(1 - 2\phi)}{\delta^2} \right] \tag{6}$$

where $|\nabla \phi| = \phi (1 - \phi) / \delta$.

The present diffuse-interface model for Hele–Shaw flow is derived from the two-phase model of Ref. [8] in the same manner as the standard sharp-interface Hele–Shaw model of Section 2.1 is derived from the full Navier–Stokes equations. A parabolic velocity profile is assumed across the gap width b, the equations are averaged across the gap, and the averaged equations are rescaled [12] under the condition that $b \ll L$. Employing the same assumptions as stated in the previous sub-section, the resulting diffuse-interface continuity and momentum equations are given by

$$\frac{\partial \phi_k}{\partial t} + \nabla \cdot (\phi_k \mathbf{u}_k) = 0 \tag{7}$$

$$\mathbf{u}_k = -\frac{b^2}{12\mu_k} \left[\nabla p_k + \sigma \delta \phi_j \nabla \left(\frac{\nabla^2 \phi_k}{\phi_k \phi_j} \right) - \rho_k \mathbf{g} \right] \tag{8}$$

where $\phi_1 = 1 - \phi_2 = \phi$ and the subscript j denotes the phase that is not phase k. The second term inside the square brackets of Eq. (8) is the capillary stress gradient in phase k and is non-zero only inside the diffuse interface. The interfacial mass balance is trivial in the absence of phase change, while the diffuse-interface version of the interfacial momentum balance, Eq. (4), is given by [8]

$$p_1 - p_2 = -\sigma \delta \frac{\nabla^2 \phi}{\phi (1 - \phi)}. \tag{9}$$

Eqs. (7) to (9) are valid everywhere in the domain and can be solved for the phase-field, ϕ, and the individual phase velocities, $\mathbf{u}_k$, and pressures, p_k.

Additional insight and some simplification in the solution can be gained by rewriting the above equations in terms of a mixture density, ρ, a mixture velocity, $\mathbf{u}$, a slip velocity, $\Delta \mathbf{u}$, a mixture pressure, p, and a mixture viscosity, μ. These variables are defined, respectively, as

$$\rho = \rho_1 \phi + \rho_2 (1 - \phi) \tag{10}$$

$$\mathbf{u} = \left[\rho_1 \phi \mathbf{u}_1 + \rho_2 (1 - \phi) \mathbf{u}_2 \right] / \rho \tag{11}$$

$$\Delta \mathbf{u} = \mathbf{u}_1 - \mathbf{u}_2 \tag{12}$$

$$p = p_1 \phi + p_2 (1 - \phi) \tag{13}$$

$$\mu = \mu_1 \phi + \mu_2 (1 - \phi) \tag{14}$$

Introducing these variables into Eqs. (7) and (8), the two-phase diffuse-interface model can be rewritten as

$$\frac{\partial \phi}{\partial t} + \mathbf{u} \cdot \nabla \phi = -\rho \nabla \cdot \left(\frac{\phi (1 - \phi)}{\rho} \Delta \mathbf{u} \right) \tag{15}$$

$$\nabla \cdot \mathbf{u} = (\rho_1 - \rho_2) \nabla \cdot \left[\frac{\phi (1 - \phi)}{\rho} \Delta \mathbf{u} \right] \tag{16}$$

$$\mathbf{u} = -\frac{b^2}{12\mu} k_{rel} \left[\nabla p + \frac{\sigma \delta}{\phi (1 - \phi)} \nabla^2 \phi \nabla \phi - B \rho \mathbf{g} \right] \tag{17}$$

$$\Delta \mathbf{u} = -\frac{b^2}{12} \frac{\mu_2 - \mu_1}{\mu_1 \mu_2} \left[\nabla p + \frac{\sigma \delta}{\phi (1 - \phi)} \nabla^2 \phi \nabla \phi \right]$$
$$+ \frac{b^2}{12} \frac{\rho_1 \mu_2 - \rho_2 \mu_1}{\mu_1 \mu_2} \mathbf{g} \tag{18}$$

where the relative "permeability", k_{rel}, and the relative "kinetic" density, B, in Eq. (17) are given by

$$k_{rel} = 1 + \frac{(\rho_2 \mu_1 - \rho_1 \mu_2)(\mu_1 - \mu_2)}{\rho \mu_1 \mu_2} \phi (1 - \phi) \tag{19}$$

$$B = 1 + \frac{(\rho_2 - \rho_1) \mu (\rho_2 \mu_1 - \rho_1 \mu_2) \phi (1 - \phi)}{\rho^2 \mu_1 \mu_2 + \rho (\rho_2 \mu_1 - \rho_1 \mu_2)(\mu_1 - \mu_2) \phi (1 - \phi)}. \tag{20}$$

The two factors given by Eqs. (19) and (20) are different from unity only inside the diffuse interface, and $k_{rel} = 1$ for $\mu_1 = \mu_2$ and $B = 1$ for $\rho_1 = \rho_2$.

It is emphasized again that Eqs. (15) to (18) are mathematically equivalent to Eqs. (7) and (8). Even though Eqs. (15) to (18) are written in terms of mixture variables, the individual phase velocities and pressures inside of the diffuse interface are not assumed equal. In other words, Eqs. (15) to (18) still constitute a full two-phase model. The following additional observations can be made. The continuity equations, Eqs. (15) and (16), feature terms on the right-hand side that are non-zero only inside of the diffuse interface. Both of these "source" terms can be attributed to the presence of a velocity slip, $\Delta\mathbf{u}$. The source term in Eq. (15) indicates that the phase-field, ϕ, is not only advected by the mixture flow, but is also changed by slip velocity gradients. The source term in Eq. (16) shows that the mixture velocity field inside the diffuse interface is non-solenoidal in the presence of slip velocity gradients; however, this term vanishes if the densities of the two phases are the same. The term $\sigma\delta\nabla^2\phi\nabla\phi/\phi(1-\phi)$ in the momentum equation, Eq. (17), represents the diffuse-interface surface tension force per unit volume and is equivalent to the capillary stress term in diffuse-interface models that are based on thermodynamic or continuum theories [1,6]. Eq. (18) shows that the slip velocity is non-zero only in the presence of viscosity and/or density differences between the phases. Finally, note that only the mixture pressure, p, appears in Eqs. (15) to (18). Hence, knowledge of the individual phase pressures, p_k, is not necessary for the solution of this set of equations. If so desired, the phase pressures can be calculated from the mixture pressure by combining Eqs. (9) and (13).

A true mixture diffuse-interface model, where the velocities and pressures inside of the diffuse interface are assumed equal (see Fig. 2), can be obtained from Eqs. (15) to (18) by setting $\Delta\mathbf{u} = 0$ and $k_{rel} = B = 1$. The resulting set of governing equations is given by

$$\frac{\partial\phi}{\partial t} + \mathbf{u}\cdot\nabla\phi = 0 \tag{21}$$

$$\nabla\cdot\mathbf{u} = 0 \tag{22}$$

$$\mathbf{u} = -\frac{b^2}{12\mu}\left[\nabla p + \frac{\sigma\delta}{\phi(1-\phi)}\nabla^2\phi\nabla\phi - \rho\mathbf{g}\right]. \tag{23}$$

In the following sections, the above mixture model, Eqs. (21) to (23), is compared to the two-phase model, Eqs. (15) to (18). Note that for both models, the diffuse-interface thickness measure δ is a free parameter.

2.3. Phase-field equation

In the present diffuse-interface model, the motion of the phase-field, ϕ, is governed by the continuity equation, Eq. (15). In other words, interface motion is not curvature driven, even though curvature plays an important role in the capillary stress term in the momentum equation. It is important to note that Eq. (15) is a hyperbolic equation that propagates any function ϕ with the flow. Therefore, special procedures are needed to ensure that the hyperbolic tangent phase-field profile across the diffuse interface, Eq. (5), is recovered as the stationary solution of Eq. (15). This issue was first addressed by Folch et al. [4], who introduced a so-called "counter-term" into their phase-field equation to cancel out curvature-driven interface motion while maintaining a hyperbolic tangent phase-field profile across the interface as the stationary solution. This approach was further investigated by Sun and Beckermann [10], who performed detailed numerical studies of the ability of such a phase-field equation to accurately track various interface motions. They found that the accuracy and robustness (e.g., in the presence of interface singularities) of the phase-field method is as good as or better than that of the standard level-set or VOF methods for interface tracking. Hence, the method of Ref. [10] is adopted here.

The phase-field equation used in the present study is given by [10]

$$\frac{\partial\phi}{\partial t} + \mathbf{u}\cdot\nabla\phi = -\rho\nabla\cdot\left(\frac{\phi(1-\phi)}{\rho}\Delta\mathbf{u}\right)$$

$$- b\left[\nabla^2\phi - \frac{\phi(1-\phi)(1-2\phi)}{\delta^2} - |\nabla\phi|\nabla\cdot\left(\frac{\nabla\phi}{|\nabla\phi|}\right)\right] \tag{24}$$

where b is a numerical parameter. The term in the square brackets on the right-hand side of Eq. (24) is added to the continuity equation, Eq. (15), to sustain the hyperbolic tangent ϕ profile across the diffuse interface during motion. The last term in the square brackets is the so-called counter-term [4] that cancels out curvature-driven interface motion at leading order for a finite interface width [see also Eq. (6)]. For a flat interface where $\kappa = 0$, the last term in the square brackets is equal to zero and the first two terms (i.e. $\nabla^2\phi - \phi(1-\phi)(1-2\phi)/\delta^2$) yield the hyperbolic tangent ϕ profile as the stationary solution of Eq. (24). During interface motion, the term in the square brackets sustains the hyperbolic tangent ϕ profile, while the $\nabla^2\phi$ term smoothes out interface singularities. Note that for the mixture diffuse-interface model where $\Delta\mathbf{u} = 0$, the first term on the right-hand side of Eq. (24) vanishes.

Eq. (24) is solved numerically using the procedures described in Ref. [10]. The discretization employs a standard explicit finite-difference method together with a fourth-order convex essentially non-oscillatory (CENO) scheme for the hyperbolic $\mathbf{u}\cdot\nabla\phi$ term. The reader is also referred to Ref. [10] for a method to choose an optimum value for the numerical parameter b in Eq. (24) as a function of the time step and the node spacing.

3. One-dimensional test cases

The model is first tested for three simple one-dimensional problems involving a stationary interface between the two phases. The first two problems are concerned with pressure-driven and buoyancy-driven flows parallel to a planar interface. These cases are used to examine the performance of the present two-phase diffuse-interface model for large viscosity and density contrasts between the phases. The third test problem is for a spherical interface in static equilibrium and is used to explain the capillary stress term in the momentum equations. In all three cases, Eq. (5) is used as the stationary phase-field profile across the interface.
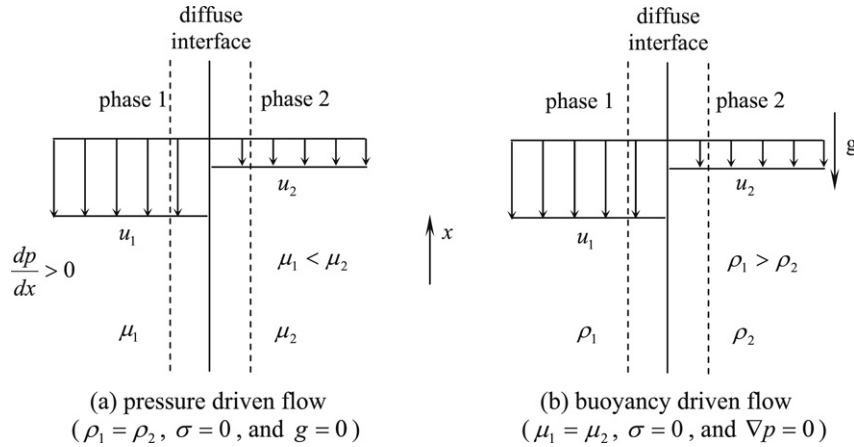
3.1. Two-phase pressure-driven flow parallel to a planar interface

Consider two fluids of different viscosity, but equal density, separated by a planar stationary interface, as illustrated in Fig. 4(a). The flow in both fluids is driven by a constant pressure gradient parallel to the interface, i.e. $dp/dx = \text{const}$. Surface tension and gravity are absent. For a sharp interface, the exact solution to this problem is given by constant velocities in each fluid with a slip at the interface, i.e.
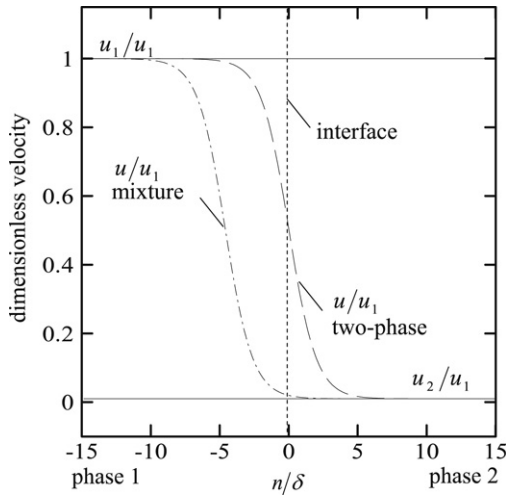
$$u_1 = -\frac{b^2}{12\mu_1}\frac{dp}{dx} \quad\text{and}\quad u_2 = -\frac{b^2}{12\mu_2}\frac{dp}{dx} = \frac{u_1\mu_1}{\mu_2} = \frac{u_1}{r_\mu} \tag{25}$$

where the viscosity ratio is given by $r_\mu = \mu_2/\mu_1$. For the present case, the solution of the two-phase diffuse-interface model is identical to the above sharp-interface solution. This can be seen easily from Eq. (8) by setting $\sigma = 0$ and $g = 0$. The mixture and slip velocities are obtained from Eqs. (17) and (18) as

$$u = u_1\phi + u_2(1-\phi) = -\frac{b^2}{12\mu}k_{rel}\frac{dp}{dx} \tag{26}$$

Fig. 4. Schematic illustrations of the one-dimensional test cases for two-phase Hele–Shaw flows.

(a) pressure driven flow
($\rho_1 = \rho_2$, $\sigma = 0$, and $g = 0$)

(b) buoyancy driven flow
($\mu_1 = \mu_2$, $\sigma = 0$, and $\nabla p = 0$)

Fig. 5. Calculated velocity profiles for the two-phase pressure-driven flow illustrated in Fig. 4(a) for all three models at $r_\mu = 100$.

and

$$\Delta u = u_1 - u_2 = -\frac{b^2}{12} \frac{(\mu_2 - \mu_1)}{\mu_1 \mu_2} \frac{dp}{dx} = u_1 \left(1 - \frac{1}{r_\mu}\right) \qquad (27)$$

where $\mu = \mu_1 \phi + \mu_2 (1 - \phi)$ and $k_{rel} = 1 + \frac{(\mu_1 - \mu_2)^2}{\mu_1 \mu_2} \phi (1 - \phi)$. Eq. (27) shows that the slip velocity is independent of ϕ and equal to the expression given by the sharp-interface solution, Eq. (25). The solution of the mixture model ($\Delta u = 0$) for a diffuse interface is given by Eq. (26) with $k_{rel} = 1$.

Fig. 5 shows a comparison of the above solutions for a viscosity ratio of $r_\mu = 100$. The mixture velocity profile corresponding to the two-phase model, as given by Eq. (26), is symmetric with respect to the interface (or $\phi = 0.5$) and follows the hyperbolic tangent variation of the phase-field profile across the interface. This smearing of the mixture velocity has no effect on the accuracy of the solution of the two-phase model. As already mentioned, the solution of the two-phase diffuse-interface model for u_1 and u_2 is identical to the sharp-interface solution, regardless of the thickness of the diffuse interface. On the other hand, the mixture velocity profile for the mixture model, as given by Eq. (26) with $k_{rel} = 1$, is strongly shifted towards the less viscous fluid (phase 1) and can be considered highly inaccurate. Only for a diffuse-interface thickness approaching zero would this shift become tolerable. Hence, this simple example illustrates the main drawback of standard diffuse-interface models where the mixture viscosity is specified as the

mean of the individual phase viscosities. The present two-phase model, allowing for a slip velocity inside of the diffuse interface, does not suffer from this shortcoming and provides the exact solution for any viscosity ratio and any diffuse-interface thickness.

3.2. Two-phase buoyancy-driven flow parallel to a planar interface

Consider two fluids of different density, but equal viscosity, separated by a planar stationary interface, as illustrated in Fig. 4(b). The flow in both fluids is driven by gravity that is acting parallel to the interface. Surface tension and pressure gradients are absent. For a sharp-interface, the exact solution to this problem is again given by constant velocities in each fluid with a slip at the interface, i.e.

$$u_1 = -\frac{b^2}{12\mu} \rho_1 g \quad \text{and} \quad u_2 = -\frac{b^2}{12\mu} \rho_2 g = \frac{u_1 \rho_2}{\rho_1} = u_1 r_\rho \qquad (28)$$

where the density ratio is given by $r_\rho = \rho_2 / \rho_1$. For the present case, the solution of the two-phase diffuse-interface model is identical to the above sharp-interface solution. This can be seen easily from Eq. (8) by setting $\sigma = 0$ and $\nabla p_k = 0$. The mixture and slip velocities are obtained from Eqs. (17) and (18) as

$$u = \frac{\rho_1 u_1 \phi + \rho_2 u_2 (1 - \phi)}{\rho} = -\frac{b^2}{12\mu} B \rho g \qquad (29)$$

and

$$\Delta u = u_1 - u_2 = \frac{b^2}{12\mu} (\rho_1 - \rho_2) g = u_1 (r_\rho - 1) \qquad (30)$$

where $\rho = \rho_1 \phi + \rho_2 (1 - \phi)$ and $B = 1 + \frac{(\rho_1 - \rho_2)^2}{\rho^2} \phi (1 - \phi)$. Eq. (30) shows that the slip velocity is independent of ϕ and equal to the expression given by the sharp-interface solution, Eq. (28). The solution of the mixture model ($\Delta u = 0$) for a diffuse interface is given by Eq. (29) with $B = 1$.

Fig. 6 shows a comparison of the above solutions for a density ratio of $r_\rho = 100$. The mixture velocity profile corresponding to the two-phase model, as given by Eq. (29), is strongly shifted towards the less dense fluid (phase 1). This shift is simply a consequence of the mixture velocity being density weighted [see Eq. (29)] and has no effect on the accuracy of the solution of the two-phase model. As already mentioned, the solution of the two-phase diffuse-interface model for u_1 and u_2 is identical to the sharp-interface solution, regardless of the thickness of the diffuse interface. On the other hand, the mixture velocity profile for the mixture model, as given by Eq. (29) with $B = 1$, is symmetric about the interface (i.e. $\phi = 0.5$). However, this symmetry is incorrect and should not be taken
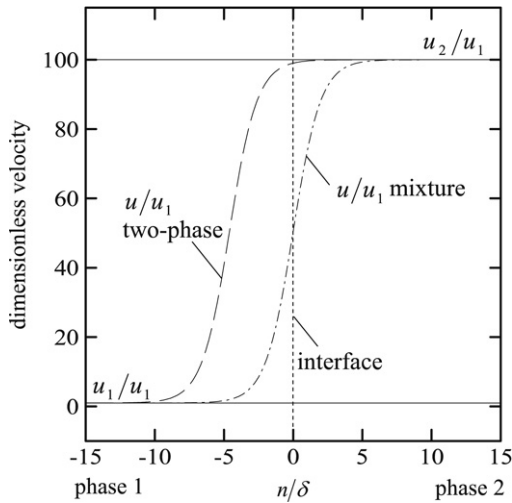
Fig. 6. Calculated velocity profiles for the two-phase buoyancy-driven flow illustrated in Fig. 4(b) for all three models at $r_\rho = 100$.

Fig. 7. Calculated pressure profiles across a spherical [with $\kappa = 1/(6\delta)$] interface for both the two-phase and mixture models.

as an indication of the accuracy of the mixture model. Only for a diffuse-interface thickness approaching zero would the correct (and shifted) mixture velocity profile be obtained. The present two-phase model, on the other hand, provides the exact solution for any density ratio and any diffuse-interface thickness.

3.3. Spherical interface in static equilibrium

Consider a spherical interface of curvature κ separating two phases. The phases are assumed to be stationary ($u = 0$) and gravity is neglected. For a sharp interface, the pressure is uniform within each phase and the pressure jump at the interface is given by $p_1 - p_2 = \sigma\kappa$. For simplicity, the far-field pressure in phase 2 ($\phi = 0$) is assumed to be equal to zero in the following. For a diffuse interface, the momentum equation, Eq. (17), reduces to

$$0 = \nabla p + \frac{\sigma\delta}{\phi(1-\phi)}\nabla^2\phi\nabla\phi. \tag{31}$$

The solution of Eq. (31) for a spherical interface, and $p(\phi = 0) = 0$, is given by [8]

$$p = p_1\phi + p_2(1-\phi) = \sigma\kappa\phi - \frac{\sigma}{\delta}\phi(1-\phi). \tag{32}$$

Note that Eq. (31) and the solution for the mixture pressure, p, given by Eq. (32) are equally valid for the two-phase and mixture models. For the two-phase model, the solution for the pressure difference between the two phases can be obtained from Eq. (9) as [8]

$$p_1 - p_2 = \sigma\kappa - \frac{\sigma}{\delta}(1-2\phi). \tag{33}$$

Note that the above solutions for the pressures depend on the diffuse-interface thickness parameter, δ. As the previous two test cases illustrate, such a dependence of the solution on δ does not exist for the two-phase model in the absence of surface tension.

Fig. 7 shows the above solutions for a spherical interface. The pressures are non-dimensionalized with $\sigma\kappa$. In this example, the interface thickness is taken to be $\delta = (6\kappa)^{-1}$. As expected, the dimensionless mixture pressure varies continuously from unity in phase 1 to zero in phase 2. Inside of the diffuse interface, the dimensionless mixture pressure experiences an inverse hump. The depth of the hump at $\phi = 0.5$ increases with decreasing diffuse-interface thickness, such that for an infinitely thin diffuse interface, the pressure at $\phi = 0.5$ would approach negative
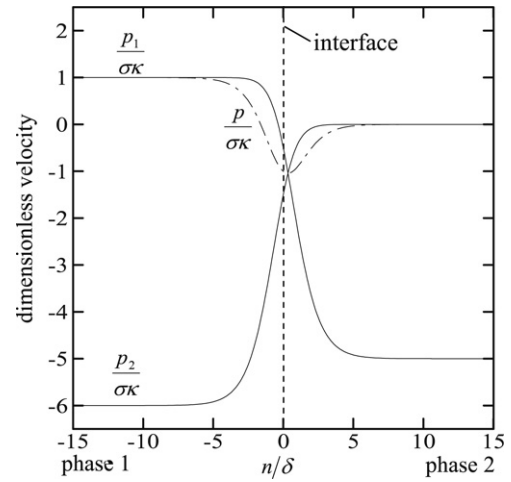
infinity. This hump is a direct consequence of the capillary stress term in the momentum equation and is present in all diffuse-interface models of two-phase flows with surface tension [6]. Note from Eq. (33) that the hump is present even for a flat interface with $\kappa = 0$. In a numerical solution, the hump needs to be accurately resolved, which becomes increasingly difficult for a decreasing diffuse-interface thickness. Fig. 7 also shows the variations of the individual phase pressures, p_1 and p_2, for the present two-phase model. The pressures of each phase feature steep variations inside of the diffuse interface and approach constant values within each phase. However, these phase pressure variations play no role in the solution of the present two-phase model, since the knowledge of the mixture pressure alone is sufficient to solve the set of governing equations.

4. Buoyancy-driven Rayleigh–Taylor instability

### 4.1. Problem description and model validation

The present diffuse-interface model is used to simulate buoyancy-driven flow and Rayleigh–Taylor instability of fluid layers inside a Hele–Shaw cell. The model is validated by comparing the predicted interface evolution, before any topology changes occur, to available results from a sharp-interface model. The dependence of the results on the diffuse-interface width is also investigated.

The physical problem considered is adopted from Lee et al. [3]. As illustrated in Fig. 3, an unstable stratification is introduced by surrounding a layer of a light fluid, phase 1, by a heavy fluid, phase 2. The initial location of the interfaces is given by $(x, y_1(x, 0))$ and $(x, y_2(x, 0))$, where [3]

$$\begin{cases} y_1(x, 0) = \pi - (0.5 + 0.1\cos x) \\ y_2(x, 0) = \pi + (0.5 + 0.1\cos x) \end{cases} \quad 0 \le x \le 2\pi. \tag{34}$$

Here, x and y are non-dimensionalized by $L_0 = L/2\pi$. Periodic boundary conditions are applied in both the x and y directions. Under gravity, the upper interface is unstable and the upper heavy fluid flows downwards through the layer of light fluid. The lower interface is stable and resists motion. Ultimately, the two interfaces meet and pinch off.

For this problem, the two-phase and mixture diffuse-interface equations listed in Section 2.2 are non-dimensionalized using L_0, $t_0 = \mu_2 L/2\pi b^2 (\rho_1 - \rho_2) g$, $u_0 = L_0/t_0$, and $p_0 = (\rho_1 - \rho_2)gL/2\pi$ as the length, time, velocity, and pressure scales, respectively. Two dimensionless parameters, the Bond number,
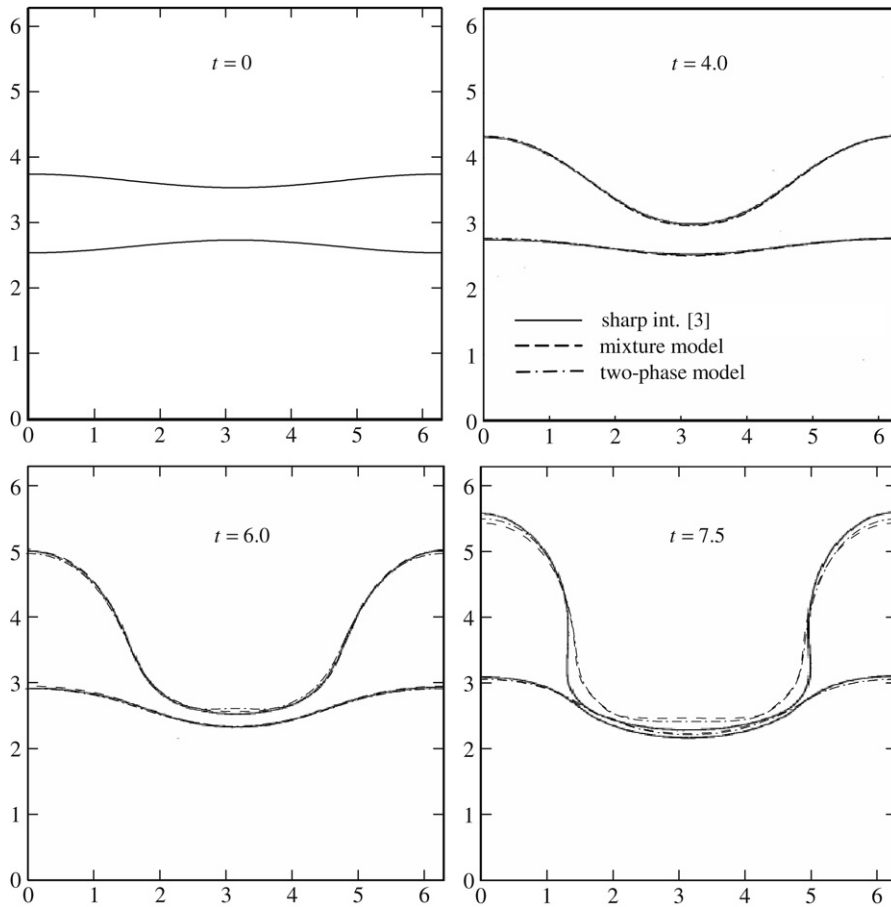
Fig. 8. Evolution of interfaces: comparison between sharp- and diffuse-interface solutions ($r_\rho = 0.9$, $r_\mu = 1.0$, $Bo = 25$, and $\delta = 0.04$).
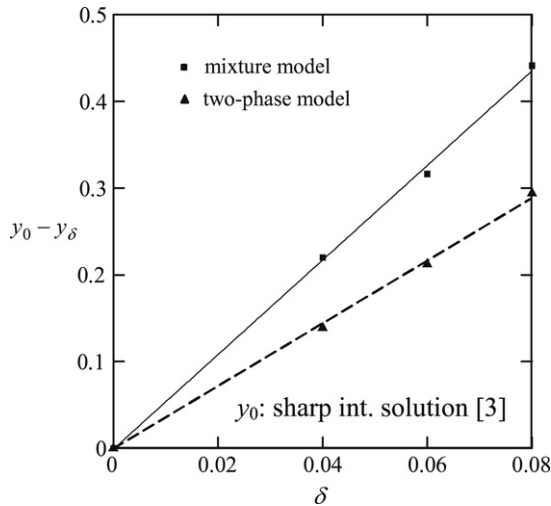
Fig. 9. Convergence of y intercept of the upper interface at $t = 7.5$ wrt. δ ($r_\rho = 0.9$, $r_\mu = 1.0$, and $Bo = 25$). Here, y_0 is from the sharp-interface solution of Ref. [3] and y_δ corresponds to the diffuse-interface solution for different interface widths δ.

$Bo = (\rho_1 - \rho_2) g (L/2\pi)^2 / \sigma$, and the Atwood number, $At = (\mu_2 - \mu_1) / (\mu_2 + \mu_1)$, characterize the interface motion [2–5]. Symbols denoting dimensionless variables are dropped in the following.

A pressure Poisson equation can be obtained by substituting Eqs. (17) and (18) into Eq. (16), and solved numerically using the pre-conditioned conjugate gradient method [13]. Once the pressure field is determined, the mixture velocity and the slip velocity are calculated explicitly using Eqs. (17) and (18). The

numerical implementation of the present models is validated by comparing the predictions to the boundary-integral, sharp-interface solution provided by Lee et al. [3]. The values of the governing parameters for the validation case are: density ratio $r_\rho = \rho_1/\rho_2 = 0.9$, viscosity ratio $r_\mu = \mu_1/\mu_2 = 1$, and $Bo = 25$. The mesh size used in the numerical solution of the diffuse-interface model is 250×250 grid points and the interface width used is $\delta = 0.04$. The calculated interface contours before pinch-off (at $t = 0$, 4, 6, and 7.5) for both the two-phase and mixture diffuse-interface models are presented in Fig. 8 and compared with those of the sharp-interface solution of Ref. [3]. Note that a boundary-integral solution cannot be obtained during and after pinch-off. It can be seen from Fig. 8 that the results from the present two-phase and mixture models almost overlap. This can be expected because in this example the viscosity ratio is equal to unity and the density ratio is close to unity. The diffuse-interface results are in good agreement with the sharp-interface solution, except near the pinch-off time (i.e., at $t = 7.5$). At that time, the diffuse interfaces are starting to overlap. Similar differences between diffuse- and sharp-interface results near the pinch-off have also been observed by Lee et al. [3].

The differences between the diffuse- and sharp-interface results before pinch-off can be attributed to the diffuse-interface predictions not being fully converged with respect to the interface width, δ. Identical results can only be expected for $\delta \rightarrow 0$. Fig. 9 shows the convergence behavior of the two-phase and mixture diffuse-interface models with respect to δ. The calculated y intercept of the upper interface (i.e., the $\phi = 0.5$ contour), y_δ, at $t = 7.5$ is used as the figure of merit. The reference intercept, y_0, is obtained from the sharp-interface solution of Ref. [3]. It can be seen that for a finite interface width, the calculated y_δ at $t = 7.5$

Fig. 10. Evolution of phase-field contours ($\phi = 0.1, 0.3, 0.5, 0.7$, and 0.9) near the pinch-off: comparison of the two-phase and mixture diffuse-interface models ($r_\rho = 0.01$, $r_\mu = 0.1$, $Bo = 25$, $At = 0.82$, and $\delta = 0.04$).

can differ significantly from the sharp-interface result. The two-phase and mixture diffuse-interface models show both a linear convergence behavior with respect to δ, and the sharp-interface solution is indeed approached for $\delta \to 0$. However, for a given interface width, more accurate results are obtained by the two-phase model, even though the density contrast is small and $r_\mu = 1.0$ in this case.

4.2. Results for large property contrasts between phases

The two-phase and mixture ($\Delta \mathbf{u} = 0$) diffuse-interface models can be expected to differ more significantly for large property contrasts between the two phases. Hence, additional simulations

were conducted for density and viscosity ratios of $r_\rho = 0.01$ and $r_\mu = 0.1$ between the phases. These ratios correspond to a much less dense and less viscous phase 1 (middle fluid layer) compared to phase 2. The Bond number is kept unchanged (i.e., $Bo = 25$) by adjusting g. The focus in the following discussion is on (i) the topology transition around the pinch-off time and (ii) the convergence of the results with respect to the diffuse-interface width.

Calculated phase-field contours at various times for the case of $r_\rho = 0.01$ and $r_\mu = 0.1$ are shown in Fig. 10 for both the two-phase and mixture models. It can be seen that the pinch-off occurs earlier for the two-phase model than for the mixture model. Also, at $t = 2.0$, two satellite drops appear for the two-phase model, while